# Purification and Improved Nuclear Radiation Detection of $Tl_6SI_4$ Semiconductor

Wenwen Lin,[†,※] Zhifu Liu,[‡] Constantinos C. Stoumpos,[†] Sanjib Das,[‡] Yihui He,[†] Ido Hadar,[†] John A. Peters,[‡] Kyle M. McCall,[†,‡] Yadong Xu,[†] Duck Young Chung,[※] Bruce W. Wessels,[‡] and Mercouri G. Kanatzidis[†,*]

[†]Department of Chemistry and [‡]Department of Materials Science and Engineering, Northwestern University, Evanston, Illinois 60208, United States

[※]Materials Science Division, Argonne National Laboratory, Lemont, Illinois 60439, United States

**ABSTRACT:** The wide bandgap semiconductor $Tl_6SI_4$ (2.14 eV) has high photon stopping power and is a promising material for detecting X-rays. In order to improve its photoresponse to low-flux $\gamma$-rays, material purification prior to crystal growth is crucial. In this contribution, we report effective purification protocols, impurity analysis followed by synthesis and crystal growth, charge transport and detector performance of large-size $Tl_6SI_4$ crystals. Purification methods of evaporation and zone refining were developed, and their high effectiveness was confirmed by impurity analysis via glow discharge mass spectrometry. Centimeter-size single crystals were the grown using the Bridgman method. The improved properties after material purification were confirmed by photoluminescence measurements. The energy of valance band maximum of a $Tl_6SI_4$, measured with photoemission spectroscopy in air (PESA) is ~5.34 ± 0.05 eV. Detector devices fabricated from the single crystal exhibit a high resistivity of $5 \times 10^{12}$ Ω·cm. The detector shows promising photoresponse under 22.4 keV Ag K$\alpha$ X-rays and 122 keV $\gamma$-rays from $^{57}$Co. Spectroscopic energy resolution was achieved for 5.5 MeV $\alpha$-particles from $^{241}$Am radiation source with a full width at half maximum of 27% at an electric field intensity of 2500 V·cm$^{-1}$. On the basis of its spectral response to $^{57}$Co $\gamma$-rays, the electron mobility-lifetime product $\mu_e\tau_e$ was estimated as $1.4 \times 10^{-5}$ cm$^2$·V$^{-1}$. Drift mobility measurements via a time of flight technique using spectral photoresponse induced by $\alpha$-particles reveal a high electron mobility of 35 ± 7 cm$^2$·V$^{-1}$·s$^{-1}$.

## ■INTRODUCTION

New wide-band-gap semiconductors with high resistivity and high photon stopping power are needed for nuclear radiation detection applications at room temperature. Compared with the classic scintillator detectors coming with large photomultiplier tubes,[1] semiconductor detectors can achieve efficient photo-electric conversion with linear responses to the energy of the nuclear radiation. The ideal semiconductor for nuclear radiation detection should simultaneously meet a number of physical properties including i) sufficiently high bandgap for suppressing carrier ionization at room temperature, ii) high average atomic number ($Z$) to guarantee high photon stopping power, iii) high carrier mobility-lifetime product $\mu\tau$ to allow for spectroscopic-grade performance, iv) low-density of deep levels with small capture cross setions,[2] v) availability of large-size and high-quality single crystals, and vi) robust mechanical properties for material processing.[3-5] The leading semiconductor material in the field of gamma-ray radiation detection, $Cd_{0.9}Zn_{0.1}Te$ (CZT),[6] still suffers from issues regarding its intrinsic defects, poor uniformity in composition and Te precipitates, twinning, resulting to a high product cost.[7-8] TlBr is another high performance detector material with high electron mobility-lifetime product ($\mu\tau$) of ~$10^{-3}$ $cm^2 \cdot V^{-1}$ ,[9-12] but is limited in device applications by intrinsic polarization-induced instability.[3, 13] Therefore, the demands on developing alternative high-quality and high-performance semiconductor detection materials have not yet been met.

Our previous studies of hybrid chalcohalide ternary compounds or halide compounds for hard radiation detection have identified several promising materials, $Tl_6SI_4$, $Tl_6SeI_4$, $Hg_3Se_2Br_2$, $CuISe_3$ and SbSeI.[14-27] Ternary halides are also very promising including $TlSn_2I_5$ and $CsPbBr_3$. [28-30] In this report we focus on $Tl_6SI_4$ crystallizing in the tetragonal $P4/mnc$ space group, with lattice parameters of $a$ = 9.1758(13) Å, $c$ = 9.5879(19) Å, $V$ = 807.32(2) $Å^3$, [16] as shown in Figure 1a and 1b. $Tl_6SI_4$ possesses a high average atomic number of 66 and a density of 7.265 $g \cdot cm^{-3}$ which provide a superior photon stopping power, compared to those of CZT with a density of 5.78 $g \cdot cm^{-3}$ and an average $Z$ of 49 (Figure 1c).[31] $Tl_6SI_4$ has a wide bandgap of 2.14 eV and high resistivity over than $10^{10}$ Ω·cm.[16] It congruently melts at a relatively low temperature of 427 °C without any phase transitions,[16] allowing for facile material purification process, crystal growth protocols and low density of phase transition induced defects. In addition, $Tl_6SI_4$ has a relatively high static dielectric constant calculated (~19), which should favor screening of excited carriers from charged defects and impurities.[23] Because of these characteristics, detectors made of $Tl_6SI_4$ single crystals have shown good response to high-flux X-rays in our previous work.[16] However, these detectors had no response for low-flux 122 keV $\gamma$-rays from $^{57}Co$.[16] The difference in detection performance of X-rays and $\gamma$-rays stems from different electron-hole pair generation rates induced by incident photons. X-ray photoresponse measurements typically employ relatively high photon fluxes, as the estimated carrier generation rate (> $10^{18}$ pairs $\cdot s^{-1} \cdot cm^{-2}$ at a X-ray tube voltage of 40 kV and a current of 2 mA)[32] exceeds the removal rate of photocarriers under electric field by orders of magnitude. So the electronic system is in a dynamic

equilibrium but not in a thermal equilibrium. Therefore, the oversaturated electrons passivate all the active deep levels, deactivating these centers. [32] In this case, to obtain X-ray photoresponse the requirement on impurity grade is more relaxed. On the contrary, the $\gamma$-ray spectroscopy measurements usually involve photons of low fluxes, since the estimated carrier generation rate ($< 10^9$ pairs$\cdot s^{-1}\cdot cm^{-2}$) is on the same order of the removal rate of carriers under electric fields. Under these circumstances, the system is very close to thermal equilibrium which allows the active electron trapping centers to reduce charge collection efficiency. Thus, the requirement on impurity grade of raw materials is much stricter to obtain good $\gamma$-ray photoresponse, and therefore material purification prior to crystal growth is crucial.

In this contribution, the systematic material purification process, syntheses, crystal growth by Bridgman method, charge transport and detection performance of $Tl_6SI_4$ are described. The effectiveness of purification by evaporation and zone refining methods was confirmed by impurity analysis using glow discharge mass spectrometry (GDMS). A large-sized single crystal was grown by the Bridgman method,[33] and subsequently fabricated as a detector with a high resistivity of $10^{12}$ $\Omega\cdot$cm. The improved crystallinity of single crystal after material purification process was verified by photoluminescence measurements. The detector detects Ag K$\alpha$ X-rays (22.4 keV) and $\gamma$-rays from $^{57}$Co (122 keV). Spectroscopic resolution was achieved for $\alpha$-particles (5.5 MeV) from $^{241}$Am with a full width at half maximum of 27% under an electric field of 2500 V$\cdot cm^{-1}$. Drift mobility measurements through a time of flight technique reveal a high electron mobility of $35 \pm 7$ $cm^2\cdot V^{-1}\cdot s^{-1}$, which is close to one of the leading detection materials TlBr. This compound shows promise for high performance $\gamma$-ray detectors upon further material purification and stoichiometry control.

## ■ EXPERIMENTAL SECTION

**Precursor materials–purification using evaporation method and zone refining.** The precursors for the synthesis of $Tl_6SI_4$ raw material were TlI beads (5N purity, Alfa Aesar), Tl chunks (5N purity, Alfa Aesar) and S shots (99.999% purity, Alfa Aesar). An evaporation method in a bent tube was developed for purifying volatile TlI and S precursors. [27] Figure S1a in Supporting Information (SI) illustrates the principle of evaporation method in a bent tube. A quartz ampoule is flame bent in the central section, and one end of the ampoule is loaded with TlI or S to be subject to purification. The ampoule is vertically fixed into a two-zone horizontal furnace. The left half and right half of ampoule is mounted in the hot zone and cold zone, respectively. Owing to the temperature gradient between two zones, the volatile material will be transported and condense on the right half of ampoule. Figure S1b and Figure S1c show the S and TlI raw materials to be purified in bent tubes, respectively. The Table S1 in SI the shows the temperature settings for purification of S and TlI precursors in bent tubes. Since the saturated vapor pressure of Tl metal precursor is only 110 Pa at 800 ºC,[34] the purification by evaporation method is not efficient for

Tl metal. Therefore, multiple-pass zone refining was adopted to purify $Tl_2S$ precursor instead of purifying Tl metal by evaporation. $Tl_2S$ binary precursor was synthesized by mixing purified S by evaporation and Tl (5N purity, Alfa Aesar) with a molar ratio of 2:1 at 500 ºC for 1 day in a rocking furnace. The as-synthesized $Tl_2S$ polycrystalline material was then loaded into a glassy carbon boat (width: 16 mm, length: 100 mm, height: 10 mm) for further purification by zone refining. The loaded boat was then put into a fused silica tube with 21 mm inner diameter (ID) and 25 mm outer diameter (OD). The above process was performed in the $N_2$ filled glovebox to avoid the oxidation of $Tl_2S$. Finally, the silica tube was flame sealed under a vacuum pressure of around $1 \times 10^{-4}$ mbar by continuous pumping. The purification of $Tl_2S$ ingot was performed by horizontal zone refining using two traveling furnaces. Each ring-like zone refiner has a width of 5 cm heating zone which is separated by ~10 cm from the other one. The temperature was set as 550 ºC for each furnace to ensure the complete melting of $Tl_2S$ while maintaining a reasonably narrow molten width of the $Tl_2S$ ingot. In order to achieve highly effective purification, the travelling speed of the furnace was set as low as 0.5 $cm \cdot h^{-1}$. Based on the temperature profile, the temperature gradient is estimated to be 46 $ºC \cdot cm^{-1}$. purification was complete after 50-pass refining. The tip part (firstly crystallizes) of purified $Tl_2S$ ingot was typically shiny with a smooth surface, while the tail section of $Tl_2S$ ingot comes with a coarse surface. Since most of the impurities are segregated in the tail section of ingot, only the tip section of ingot with 1/3 of ingot length was chosen for impurity analysis.

**Synthesis, crystal growth, processing and characterization of $Tl_6SI_4$.** The synthesis of $Tl_6SI_4$ raw material was carried out by chemical reaction of purified TlI and $Tl_2S$ precursors with a molar ratio of 4:1 in a sealed quartz ampoule at 550 ˚C for 1 day within a rocking furnace, and then slowly cooled down to 20 ºC in 24 h. The purified TlI precursor was dired at 90 ˚C for 24 h under vacuum to eliminate surface water before synthesis of ternary compound. The soaking temperature of 550 ˚C for synthesizing $Tl_6SI_4$ is higher than its melting point, which enables thorough melting of $Tl_6SI_4$. Subsequently, the raw material was transferred into a conical-tip and carbon film-coating quartz tube with an inner diameter of 10 mm and a thickness of 1.5 mm, which was sealed using flame at a vacuum pressure of $2 \times 10^{-4}$ mbar. Warning: Because of the extreme toxicity of Tl containing materials, appropriate protection equipment should be employed when handling Tl containing precursors. The Tl containing precursors should be stored in an inner gas filled glovebox. Single crystalline boule of $Tl_6SI_4$ was grown by the vertical two-zone Bridgman method.[33] Before the actual crystallization, the ampoule was kept still in the upper hot zone (550 ˚C) of a Bridgman furnace for 12 h to ensure thorough melting of ternary compound. After the premelting, the ampoule was gradually translated from the upper hot zone to the lower cold zone at a dropping speed of 0.5 $mm \cdot h^{-1}$. The temperature of the lower cold zone was set as 200 ˚C to maintain a temperature slope of 23 $ºC \cdot cm^{-1}$. After complete crystallization, the ingot was annealed in furnace at 200 ˚C in the lower cold zone for 48 h without dropping down. Finally, the boule was slowly quenched to room

temperature in 2 days to reduce inner thermal stress induced cracks. $Tl_6SI_4$ boule was sliced along perpendicular direction to the growth direction using a diamond-blade saw. A slice cut from the middle section of boule was polished with SiC sandpapers and water-free alumina suspension with a particle size of 0.05 μm. After fine polishing with alumina suspension, no surface etching and were carried out on the polished wafer. In order to identify the phase of crystal grown, powder X-ray diffraction (PXRD) pattern of a ground specimen from boule was chosen using a Si-calibrated CPS 120 INEL diffractometer (Cu K*a* radiation $\lambda$=1.5418 Å). A Shimadzu UV-3600PC spectrophotometer was adopted to measure solid-state UV-vis-near IR diffuse reflectance spectroscopy, and $BaSO_4$ was used as the reflectance reference.

Details of impurity analysis, photoluminescence measurement, the mechanical property assessment (hardness), charge transport and X-ray photocurrent measurements, ambient pressure photoemission spectroscopy measurements and hard radiation energy spectroscopy are given in the Supporting Information section.

## ■ RESULTS AND DISCUSSION

**Impurity analysis.** Table 1 shows impurity concentrations in TlI precursor before and after material purification by our evaporation method inside a bent silica tube. The evaporation process utilizing our bent tube method effectively removed Na, Cl, Fe, Sn and Eu from TlI. This method is not effective for removing K and Br, however, Br is isoelecronic to I and should not introduce any impurity level which is resonant with the conduction band, which are believed to be less harmful to carriers. Table 2 shows that our evaporation process eliminated most of the impurities in S including Na, B, Mg, Al, Cl, K, Ca, Fe and Bi. Table 3 shows the comparison of impurity analysis for $Tl_2S$ before and after purification by 50-pass horizontal zone refining, which is highly effectiveness in removing Mg, Ni, Cu, Ag, Te, Hg, Pb and Bi (no reduction of Al impurity was observed).

**Crystal growth and characterization.** $Tl_6SI_4$ ternary raw material was synthesized by a direct chemical reaction between the TlI and $Tl_2S$ precursors after purification process with a stoichiometric combination, and then adopted for crystal growth in a vertical Bridgman furnace with two zones. Figure 2a shows the 1 centimeter-size pristine boule of $Tl_6SI_4$ under ambient light. The as-grown crystal is of pure phase as shown in Figure 2b. Figure 2c shows the optical absorption spectrum of a $Tl_6SI_4$ ground specimen indicating a sharp bandgap at 2.06 eV, in agreement with the dark-red color of the wafer. This bandgap is sufficiently wide to inhibit the formation of thermally activated mid-gap carriers, yet remains small enough to ensure high photoinduced carriers.[35-37] In addition, this material is very robust in mechanical properties, as shown from the Vickers hardness measurement (SI, Figure S2). Its Vickers hardness was estimated to be around 63 $kg \cdot mm^{-2}$, which is comparable to that (73 $kg \cdot mm^{-2}$) of the commercial semiconductor detector material CZT.[38]

**Photoluminescence.** To identify the underlying radiative recombination mechanisms and to evaluate the crystal quality, Figure 3a shows a representative PL spectrum from a $Tl_6SI_4$ single crystal under the laser intensity of 1000 $mW.cm^{-2}$ at 17 K. The PL spectrum showed a broad emission band centered at 1.6 eV, consistent with previously reported result on this compound by our group, while showing a much narrower FWHM (a FWHM value of ~ 0.15 eV compared to the previously reported value of ~ 0.18 eV).[39] Considering the bandgap of $Tl_6SI_4$ to be 2.06 eV (Figure 2c) at room temperature, this PL emission is attributed to recombination involving defects. However, the narrower PL bandwidth indicates a narrower distribution of defects and hence, improved crystal quality. The PL spectrum was resolved using two overlapping Gaussian peaks located at 1.55 and 1.62 eV, respectively, which is in excellent accordance with our previously reported results.[39] Considering that TlI precursor is much more volatile than the $Tl_2S$ precursor, these defect-associated emission bands could be caused by Tl or I vacancies in the $Tl_6SI_4$ lattice.

To look at the nature of recombination, the dependence of the PL emission on excitation intensity was measured (Figure 3b). Generally, integrated PL intensity ($I$) is related to the excitation intensity ($L$) by a power law of the form, $I \propto L^k$, where $k$ is a dimensionless exponent indicating the nature of the observed transition.[40] The values of the exponent $k$ are generally in one of the following ranges: $0 < k < 1$ or $1 < k < 2$, where the former is ascribed to donor-acceptor pair recombination (DAP) or free-to-bound recombination, and the latter is for the free- or bound-exciton emission.[40-41] The values of $k$ calculated from the dependence of the PL emission on excitation intensity, as illustrated in Figure 3c, are $(0.95 \pm 0.15)$ and $(1.09 \pm 0.05)$ for the 1.55 and 1.62 eV bands, respectively. While the PL peak located at 1.62 can be clearly attributed to bound excitonic emission, the $k$ value for the 1.55 eV band can fall above or below 1 (within the margin of error) − making it inconclusive as to the type of emission responsible for this band. However, constant peak locations with changing laser intensity (Figure 3d) confirm that both the peaks can be attributed to bound excitonic emission.

**Charge transport and detection performance.** The valance band maximum energy (VBM) of a $Tl_6SI_4$, was measured by Photoemission spectroscopy in air (PESA, AC-2, Riken-Keiki), to be $5.34 \pm 0.05$ eV, as shown in Figure S3. By subtracting the measured band gap from the VBM, the conduction band minimum (CBM), was calculated to be $3.28 \pm 0.1$ eV. The inset in Figure 4a shows the typical planar-type detector made of a 0.8 mm thick $Tl_6SI_4$ wafer with carbon paint electrodes of 1.5 mm in diameter symmetrically on both sides of the wafer. The wafer was sliced perpendicular to crystal growth direction; therefore, the applied electric field direction is parallel to the crystallization direction. There was no sign of a reactivity between carbon electrode and crystal at the interface of electrodes. The dark current of the detector was measured to assess leakage current that can cause noise in detection signals. As shown in

Figure 4a, the current-voltage (*I-V*) curve of the detector is highly linear in the bias range from -100 V to +100 V, suggesting the absence of space charge effects or ionic conductivity that are detrimental to detector performance.[42] The resistivity of the detector was estimated as $5 \times 10^{12}$ Ω·cm, which results in a low background noise for detection, compared to ~$10^{10}$ Ω·cm or higher for CZT crystals..[43] Figure 4b demonstrates the photocurrent of the detector at a bias of 100 V for 22.4 keV X-ray irradiation from a Ag K$\alpha$ source by switching the X-rays on and off. The photocurrent under X-ray irradiation is 4 orders of magnitude higher than the dark current, demonstrating the high photosensitivity of the $Tl_6SI_4$ detector to X-rays.

Figure 4c demonstrates the spectral photoresponse of $Tl_6SI_4$ detector for 122 keV $\gamma$-rays from $^{57}$Co under cathode irradiation (electron-collection) configuration. The detector shows obvious photoresponse under $\gamma$-ray irradiation that is apparently distinguished from the noise background, showing that our material purification process leads to substantially higher crystal quality than the previous study.[16] As a result, the new crystals exhibit good photoresponse to $\gamma$-rays. More importantly, the shoulder accompanying the spectral tail in Figure 4c moves to higher energy channel numbers as applied bias increases, demonstrating that the signal arising from the $\gamma$-ray source is not due to artificial effects induced by the high bias voltages. Although the $\gamma$-ray photoresponse is good, the detector is not able to resolve the characteristic peaks of the 122 keV $\gamma$-rays from $^{57}$Co radiation source. The absence of energy spectral resolution can be presumably attributed to remaining carrier trapping centers leading to low charge collection efficiency.

The single-carrier Hecht equation was used to estimate the $\mu_e\tau_e$,[44] on basis of the spectroscopy measurements under $\gamma$-rays . The Hecht equation can be expressed as follows

$$CCE(V) = \frac{Q}{Q_0} = \frac{\mu\tau V}{L^2}\left(1 - e^{-\frac{L^2}{\mu\tau V}}\right) \quad (1)$$

, where *CCE*(*V*) refers to charge collection efficiency under certain applied bias *V*, *Q* is the measured photopeak/shoulder tail channel number at applied bias *V*, *L* (0.08 cm) is the thickness of detector wafer, $Q_0$ is the calculated saturated channel number of the photopeak/shoulder tail. The $\mu_e\tau_e$ and $Q_0$ can be derived from the experimental data of *CCE*(*V*) and *Q*. As there is no spectral energy resolution observed, the maximum channel number positions instead of photopeak channel numbers were adopted to fit the Hecht equation. The derived $\mu_e\tau_e$ is ~$1.4 \times 10^{-5}$ $cm^2 \cdot V^{-1}$, see Figure 4d.

The detection performance for 5.5 MeV $\alpha$-particles from a $^{241}$Am beam without collimation with an activity of 0.9 μCi was also measured. As shown in Figure 5a, the spectral photoresponse was collected by irradiating the cathode of detector at a bias of 200 V. The signal with a broad photopeak for $\alpha$- indicates the presence of energy resolution with a FWHM of 27% at 200 V. The electron mobility ($\mu_e$) was estimated by the drift time ($t_{drift}$) of electrons induced by an $\alpha$-particle interaction close to the cathode as the electron

drifts through the whole thickness of the detector. [45-47] The $\mu_e$ can be derived by the following equation

$$\mu_e = \frac{D}{Et_{drift}} \quad (2)$$

, $D$ and $E$ are the detector thickness and the applied electric field, respectively. The electron drift time $t_{drift}$ is estimated by determining the rise time of the electron transient waveform from the preamplifier. Figure 5b illustrates typical transient pulses induced by $\alpha$-particles from $^{241}$Am under various applied biases. One hundred measurements of electron pulse rise time were carried out and averaged for each bias in order to enhance the reliability of the data. The average electron rise time was estimated as 1.68 μs at 100 V, 1.21 μs at 150 V, 0.98 μs at 200 V and 0.70 μs at 250 V, respectively. Since the attenuation of $\alpha$-particle (< 20 μm) is much smaller than the detector thickness (0.08 cm), [48] the electron drift time approximately equals the electron pulse rise time. Figure 5c shows electrons drift velocity as a function of the electric filed intensity of $Tl_6SI_4$ detector. Using Equation 2, the electron mobility of $Tl_6SI_4$ detector can be estimated to be 35 ± 7 $cm^2 \cdot V^{-1} \cdot s^{-1}$ by linear fitting, which is close to one of the main $\gamma$-ray detector material TlBr (10 - 50 $cm^2 \cdot V^{-1} \cdot s^{-1}$).[13] Since both of the $\mu_e\tau_e$ and $\mu_e$ are known, the electron lifetime can be estimated to be 0.4 μs.

## ■ CONCLUSION

In conclusion, the semiconductor $Tl_6SI_4$ is promising for nuclear radiation detection. A major advantage of this material is its low melting point and lack of phase transitions which allows centimeter-sized single-crystals with a high resistivity on the order of $10^{12}$ Ω·cm to be grown using the Bridgman method. A detector made of $Tl_6SI_4$ shows clear photonresponse to Ag Kα X-rays (22.4 keV), $^{57}$Co γ-rays (122 keV), and $^{241}$Am $\alpha$-particles (5.5 MeV). The material has a high $\mu_e$ (35 ± 7 $cm^2 \cdot V^{-1} \cdot s^{-1}$), which is comparable to those of TlBr.[11] Material purification techniques performed using the recently developed bent-tube evaporation method and zone refining is highly effective in removing most of the impurities as evidenced by GDMS analysis,[27] and the total concentration of impurities, except Br, was reduced to 3.7 ppm after purification. The reduction of impurity concentration substantially improved crystal quality and performance. These crystals exhibit photoresponse under low-flux 122 keV $^{57}$Co $\gamma$-ray irradiation and energy resolution of 27% upon 5.5 MeV $\alpha$-particles.

## ■ ASSOCIATED CONTENTS

Supporting information is available.

The temperatures settings for the hot and cold zones in the two-zone furnace and melting and boiling points of S and TlI precursors.

Purification of S and TlI by evaporation method in a bent tube.

Details of impurity analysis, photoluminescence measurement, the mechanical property assessment (hardness), charge transport and X-ray photocurrent measurements, ambient pressure photoemission spectroscopy measurements and hard radiation energy spectroscopy are given in the Supporting Information section.

## ■ AUTHOR INFORMATION


### Corresponding Author

*E-mail: m-kanatzidis@northwestern.edu

### ORCID

Wenwen Lin: 0000-0002-1627-9558

Zhifu Liu: 0000-0001-9087-111

Constantinos C. Stoumpos: 0000-0001-8396-9578

Sanjib Das: 0000-0002-5281-4458

Yihui He: 0000-0002-1057-6826

Ido Hadar: 0000-0003-0576-9321

John A. Peters: 0000-0003-2357-1909

Kyle M. McCall: 0000-0001-8628-3811

Yadong Xu: 0000-0002-1017-9337

Duck Young Chung: 0000-0002-1315-2631

Bruce W. Wessels: 0000-0002-8957-7097

Mercouri G. Kanatzidis: 0000-0003-2037-4168


### Author Contribution

M. K. conceived and supervised the project. W. L. conceived and conducted experiments on synthesis, purification, crystal growth, characterization, charge transport, detection performance, and mobility estimation. Z. L. conducted experiments on detection performance. C. S. and K. M. helped with organizing the whole manuscript. S. D. and J. P. conducted optical measurements. Y. H. conducted hardness test. I. H. conducted the ambient pressure photoemission spectroscopy measurement. D. C. helped with material purification. B. W. supervised the charge transport measurements.

### Notes

The authors declare no competing financial interest.

## ■ ACKNOWLEDGEMENTS

This work was supported by the Department of Homeland Security ARI program with grant 2014-DN-077-ARI086-01. This work made use of the EPIC facility of the *NUANCE* Center and IMSERC at Northwestern University, which has received support from the Soft and Hybrid Nanotechnology Experimental (SHyNE) Resource (NSF NNCI-1542205). Purification by the zone refining method and crystal growth were performed at Argonne National Laboratory supported by the Department of Energy, National Nuclear Security Administration, Office of Defense Nuclear Nonproliferation Research and Development under contract No DE-AC02-06CH11357. We thank Paul Bennett, Alexei Churilov, Alireza Kargar, Leonard Cirignano and Handong Sun from Radiation Monitoring Devices for fruitful suggestions.

## ■ REFERENCES

(1) Pani, R.; Pellegrini, R.; Cinti, M. N.; Bennati, P.; Betti, M.; Vittorini, F.; Mattioli, M.; Trotta, G.; Cencelli, V. O.; Scafe, R.; Montani, L.; Navarria, F.; Bollini, D.; Baldazzi, G.; Moschini, G.; Rossi, P.; de Notaristefani, F., $LaBr_3$: Ce crystal: The latest advance for scintillation cameras. *Nucl. Instrum. Methods Phys. Res., Sect. A* **2007,** *572*, 268-269.

(2) Babentsov, V.; Franc, J.; Höschl, P.; Fiederle, M.; Benz, K. W.; Sochinskii, N. V.; Dieguez, E.; James, R. B., Characterization of compensation and trapping in CdTe and CdZnTe: Recent advances. *Cryst. Res. Technol.* **2009,** *44*, 1054-1058.

(3) Owens, A.; Peacock, A., Compound semiconductor radiation detectors. *Nucl. Instrum. Methods Phys. Res., Sect. A* **2004,** *531*, 18-37.

(4) Owens, A.; Peacock, A.; Bavdaz, M., Progress in compound semiconductors. *P. Soc. Photo-Opt. Ins.* **2003,** *4851*, 1059-1070.

(5) McGregor, D. S.; Hermon, H., Room-temperature compound semiconductor radiation detectors. *Nucl. Instrum. Methods Phys. Res., Sect. A* **1997,** *395*, 101-124.

(6) Zhang, F.; He, Z.; Seifert, C. E., A prototype three-dimensional position, sensitive CdZnTe detector array. *IEEE Trans. Nucl. Sci.* **2007,** *54*, 843-848.

(7) Szeles, C., Advances in the crystal growth and device fabrication technology of CdZnTe room temperature radiation detectors. *IEEE Trans. Nucl. Sci.* **2004,** *51*, 1242-1249.

(8) Milbrath, B. D.; Peurrung, A. J.; Bliss, M.; Weber, W. J., Radiation detector materials: an overview. *J. Mater. Res.* **2008,** *23*, 2561-2581.

(9) Churilov, A. V.; Ciampi, G.; Kim, H.; Cirignano, L. J.; Higgins, W. M.; Olschner, F.; Shah, K. S., Thallium Bromide Nuclear Radiation Detector Development. *IEEE Trans. Nucl. Sci.* **2009,** *56*, 1875-1881.

(10) Churilov, A. V.; Ciampi, G.; Kim, H.; Higgins, W. M.; Cirignano, L. J.; Olschner, F.; Biteman, V.; Minchello, M.; Shah, K. S., TlBr and $TlBr_xI_{1-x}$ crystals for gamma-ray detectors. *J. Cryst. Growth* **2010,** *312*, 1221-1227.

(11) Churilov, A. V.; Higgins, W. M.; Ciampi, G.; Kim, H.; Cirignano, L. J.; Olschner, F.; Shah, K. S., Purification, crystal growth and detector performance of TlBr. *Proc. SPIE* **2008,** *7079*, 70790K1-70790K8.
(12) Kim, H.; Cirignano, L.; Churilov, A.; Ciampi, G.; Higgins, W.; Olschner, F.; Shah, K., Developing larger TlBr detectors-detector performance. *IEEE Trans. Nucl. Sci.* **2009,** *56*, 819-823.
(13) Hitomi, K.; Shoji, T.; Ishii, K., Advances in TlBr detector development. *J. Cryst. Growth* **2013,** *379*, 93-98.
(14) He, Y.; Kontsevoi, O. Y.; Stoumpos, C. C.; Trimarchi, G. G.; Islam, S. M.; Liu, Z.; Kostina, S. S.; Das, S.; Kim, J.-I.; Lin, W.; Wessels, B. W.; Kanatzidis, M. G., Defect antiperovskite compounds $Hg_3Q_2I_2$ (Q = S, Se, and Te) for room-temperature hard radiation detection. *J. Am. Chem. Soc.* **2017,** *139*, 7939-7951.
(15) Wibowo, A. C.; Malliakas, C. D.; Liu, Z. F.; Peters, J. A.; Sebastian, M.; Chung, D. Y.; Wessels, B. W.; Kanatzidis, M. G., Photoconductivity in the chalcohalide semiconductor, SbSeI: a new candidate for hard radiation detection. *Inorg. Chem.* **2013,** *52*, 7045-7050.
(16) Nguyen, S. L.; Malliakas, C. D.; Peters, J. A.; Liu, Z. F.; Im, J.; Zhao, L. D.; Sebastian, M.; Jin, H.; Li, H.; Johnsen, S.; Wessels, B. W.; Freeman, A. J.; Kanatzidis, M. G., Photoconductivity in $Tl_6SI_4$: a novel semiconductor for hard radiation detection. *Chem. Mater.* **2013,** *25*, 2868-2877.
(17) Johnsen, S.; Liu, Z. F.; Peters, J. A.; Song, J. H.; Nguyen, S.; Malliakas, C. D.; Jin, H.; Freeman, A. J.; Wessels, B. W.; Kanatzidis, M. G., Thallium chalcohalides for X-ray and gamma-ray detection. *J. Am. Chem. Soc.* **2011,** *133*, 10030-10033.
(18) Li, H.; Meng, F.; Malliakas, C. D.; Liu, Z. F.; Chung, D. Y.; Wessels, B.; Kanatzidis, M. G., Mercury chalcohalide semiconductor $Hg_3Se_2Br_2$ for hard radiation detection. *Cryst. Growth Des.* **2016,** *16*, 6446-6453.
(19) Kostina, S. S.; Peters, J. A.; Lin, W.; Chen, P.; Liu, Z.; Wang, P. L.; Kanatzidis, M. G.; Wessels, B. W., Photoluminescence fatigue and inhomogeneous line broadening in semi-insulating $Tl_6SeI_4$ single crystals. *Semicond. Sci. Tech.* **2016,** *31*, 065009.
(20) Liu, Z. F.; Peters, J. A.; Wessels, B. W.; Johnsen, S.; Kanatzidis, M. G., Thallous chalcogenide ($Tl_6I_4Se$) for radiation detection at X-ray and gamma-ray energies. *Nucl. Instrum. Methods Phys. Res., Sect. A* **2011,** *659*, 333-335.
(21) Das, S.; Peters, J. A.; Lin, W.; Kostina, S. S.; Chen, P.; Kim, J.-I.; Kanatzidis, M. G.; Wessels, B. W., Charge transport and observation of persistent photoconductivity in $Tl_6SeI_4$ single crystals. *J. Phys. Chem. Lett.* **2017,** *8*, 1538-1544.
(22) Shi, H.; Lin, W.; Kanatzidis, M. G.; Szeles, C.; Du, M.-H., Impurity-induced deep centers in $Tl_6SI_4$. *J. Appl. Phys.* **2017,** *121*, 145102.
(23) Shi, H. L.; Du, M. H., Native defects in $Tl_6SI_4$: Density functional calculations. *J. Appl. Phys.* **2015,** *117*, 175701.
(24) Biswas, K.; Du, M. H.; Singh, D. J., Electronic structure and defect properties of $Tl_6SeI_4$: Density functional calculations. *Phys. Rev. B* **2012,** *86*, 144108.
(25) Lin, W.; Stoumpos, C. C.; Kontsevoi, O. Y.; Liu, Z.; He, Y.; Das, S.; Xu, Y.; McCall, K. M.; Wessels, B. W.; Kanatzidis, M. G., $Cu_2I_2Se_6$: A metal–inorganic framework wide-bandgap semiconductor for photon detection at room temperature. *J. Am. Chem. Soc.* **2018,** *140*, 1894–1899.
(26) Lin, W. W.; Kontsevoi, O. Y.; Liu, Z. F.; Das, S.; He, Y. H.; Stoumpos, C. C.; McCall, K. M.; Malliakas, C. D.; Wessels, B. W.; Kanatzidis, M. G., Improved crystal growth of $Tl_6SeI_4$ for

gamma-ray detection material by oxide impurity removal. *Cryst. Growth Des.* **2017,** *17*, 6096-6104.
(27) Lin, W. W.; Kontsevoi, O. Y.; Liu, Z. F.; Das, S.; He, Y. H.; Xu, Y. D.; Stoumpos, C. C.; McCall, K. M.; Rettie, A. J. E.; Chung, D. Y.; Wessels, B. W.; Kanatzidis, M. G., An Effective purification process for the nuclear radiation detector $Tl_6SeI_4$. *Cryst. Growth Des.* **2018,** *18*, 3484-3493.
(28) Lin, W. W.; Stoumpos, C. C.; Liu, Z. F.; Das, S.; Kontsevoi, O. Y.; He, Y. H.; Malliakas, C. D.; Chen, H. J.; Wessels, B. W.; Kanatzidis, M. G., $TISn_2I_5$, a robust halide antiperovskite semiconductor for gamma-ray detection at room temperature. *ACS Photon.* **2017,** *4*, 1805-1813.
(29) Liu, Z. F.; Peters, J. A.; Kim, J. I.; Das, S.; McCall, K. M.; Wessels, B. W.; He, Y. H.; Lin, W. W.; Kanatzidis, M. G., Noise sources and their limitations on the performance of compound semiconductor hard radiation detectors. *Nucl. Instrum. Methods Phys. Res., Sect. A* **2019,** *916*, 133-140.
(30) He, Y. H.; Liu, Z. F.; McCall, K. M.; Lin, W. W.; Chung, D. Y.; Wessels, B. W.; Kanatzidis, M. G., Perovskite $CsPbBr_3$ single crystal detector for alpha-particle spectroscopy. *Nucl. Instrum. Methods Phys. Res., Sect. A* **2019,** *922*, 217-221.
(31) Seltzer, S. M., Calculation of photon mass energy-transfer and mass energy-absorption coefficients. *Radiat. Res.* **1993,** *136*, 147-170.
(32) Bale, D. S.; Szeles, C., Nature of polarization in wide-bandgap semiconductor detectors under high-flux irradiation: Application to semi-insulating $Cd_xZn_{1-x}Te$. *Phys. Rev. B* **2008,** *77*, 035205.
(33) Bridgman, P. W., Certain physical properties of single crystals of tungsten, antimony, bismuth, tellurium, cadmium, zinc, and tin. *Proc. Am. Acad. Arts Sci.* **1925,** *60*, 305-383.
(34) Aldred A. T., P. J. N., Vapor pressures of zinc, cadmium, antimony, and thallium. *J. Chem. Eng. Data* **1963,** *8*, 3.
(35) Alig, R. C.; Bloom, S., Electron-hole-pair creation energies in semiconductors. *Phys. Rev. Lett.* **1975,** *35*, 1522-1525.
(36) Alig, R. C.; Bloom, S.; Struck, C. W., Electron-hole-pair creation energies in semiconductors. *B. Am. Phys. Soc.* **1980,** *25*, 175-175.
(37) Ozawa, L.; Hersh, H. N., Creation energy of electron-hole pairs in luminescent semiconductors. *J. Electrochem. Soc.* **1976,** *123*, C258-C258.
(38) Fu, X.; Xu, Y. D.; Xu, L. Y.; Gu, Y. X.; Jia, N. B.; Bai, W.; Zha, G. Q.; Wang, T.; Jie, W. Q., Indentation-introduced dislocation rosettes and their effects on the carrier transport properties of CdZnTe crystal. *Cryst. Eng. Comm.* **2016,** *18*, 5667-5673.
(39) Peters, J. A.; Sebastian, M.; Nguyen, S.; Liu, Z.; Im, J.; Freeman, A. J.; Kanatzidis, M. G.; Wessels, B. W., Optical investigation of defects in semi-insulating $Tl_6SeI_4$ single crystals. *Phys. Rev. B* **2014,** *90*, 035205.
(40) Schmidt, T.; Lischka, K.; Zulehner, W., Excitation-power dependence of the near-band-edge photoluminescence of semiconductors. *Phys. Rev. B* **1992,** *45*, 8989-8994.
(41) Fonoberov, V. A.; Alim, K. A.; Balandin, A. A.; Xiu, F.; Liu, J., Photoluminescence investigation of the carrier recombination processes in ZnO quantum dots and nanocrystals. *Phys. Rev. B* **2006,** *73*, 165317.
(42) Rose, A., Space-charge-limited currents in solids. *Phys. Rev.* **1955,** *97*, 1538-1544.

(43) Fochuk, P.; Nakonechnyi, I.; Kopach, O.; Verzhak, Y.; Panchuk, O.; Komar, V.; Terzin, I.; Kutnij, V.; Rybka, A.; Nykoniuk, Y.; Bolotnikov, A. E.; Camarda, G. C.; Cui, Y.; Hossain, A.; Kim, K. H.; Yang, G.; James, R. B., High-temperature treatment of In-doped CZT crystals grown by the high-pressure Bridgman method. *Proc. SPIE* **2012,** *8507*.
(44) Hecht, K., Zum Mechanismus des lichtelektrischen Primärstromes in isolierenden Kristallen. *Zeitschrift für Physik* **1932,** *77*, 235-245.
(45) Erickson, J. C.; Yao, H. W.; James, R. B.; Hermon, H.; Greaves, M., Time of flight experimental studies of CdZnTe radiation detectors. *J. Electron. Mater.* **2000,** *29*, 699-703.
(46) Sellin, P. J.; Davies, A. W.; Lohstroh, A.; Ozsan, M. E.; Parkin, J., Drift mobility and mobility-lifetime products in CdTe:Cl grown by the travelling heater method. *IEEE Trans. Nucl. Sci.* **2005,** *52*, 3074-3078.
(47) Szeles, C., CdZnTe and CdTe materials for X-ray and gamma ray radiation detector applications. *Phys. Status Solidi B* **2004,** *241*, 783-790.
(48) Knoll, G. F., *Radiation detection and measurement*. John Wiley & Sons, Inc.: 2010.

**Table 1.** Comparison of impurity concentrations (ppm, wt) in TlI starting material before and after purification by the evaporation method in a bent tube.

| Impurities | Before purification | After purification |
|---|---|---|
| **Na** | 1.5 | 1 |
| **Cl** | 1.9 | 0.63 |
| **K** | 2.4 | 2.7 |
| **Fe** | 0.02 | <0.01 |
| **Br** | 76 | 48 |
| **Sn** | 0.26 | <0.1 |
| **Eu** | 6.70 | <0.1 |

**Table 2.** Comparison of impurity concentrations (ppm, wt) of S before and after purification by the evaporation method in a bent tube.

| Impurities | Before purification | After purification |
|---|---|---|
| **Na** | 0.50 | <0.05 |
| **B** | 0.18 | <0.01 |
| **Mg** | 0.09 | <0.01 |
| **Al** | 0.09 | <0.01 |
| **Cl** | 2.00 | <0.1 |
| **K** | 0.63 | <0.1 |
| **Ca** | 3.50 | <0.1 |
| **Fe** | 0.45 | <0.01 |
| **Se** | 0.50 | 0.27 |
| **Bi** | 0.20 | <0.01 |

**Table 3.** Comparison of impurity concentrations (ppm, wt) of $Tl_2S$ before and after purification by 50-pass horizontal zone refining.

| Impurities | Before purification | After purification |
|---|---|---|
| **Mg** | 0.15 | <0.01 |
| **Al** | 1.11 | 0.9 |
| **Ni** | 0.02 | <0.01 |
| **Cu** | 4.82 | <0.01 |
| **Ag** | 6.76 | <0.05 |
| **Te** | 17.61 | <0.5 |
| **Hg** | 12.05 | <0.5 |
| **Pb** | 19.46 | 3 |
| **Bi** | 6.49 | 1 |

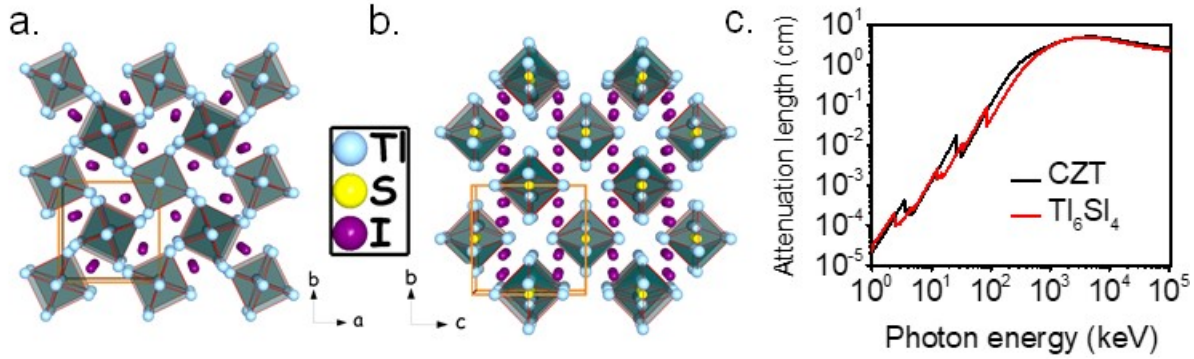


**Figure 1.** Crystal structure of $Tl_6SI_4$ in **(a)** the *c* direction and **(b)** *a* direction. **(c)** Estimated attenuation lengths for CZT and $Tl_6SI_4$ as a function of incident photon energy.

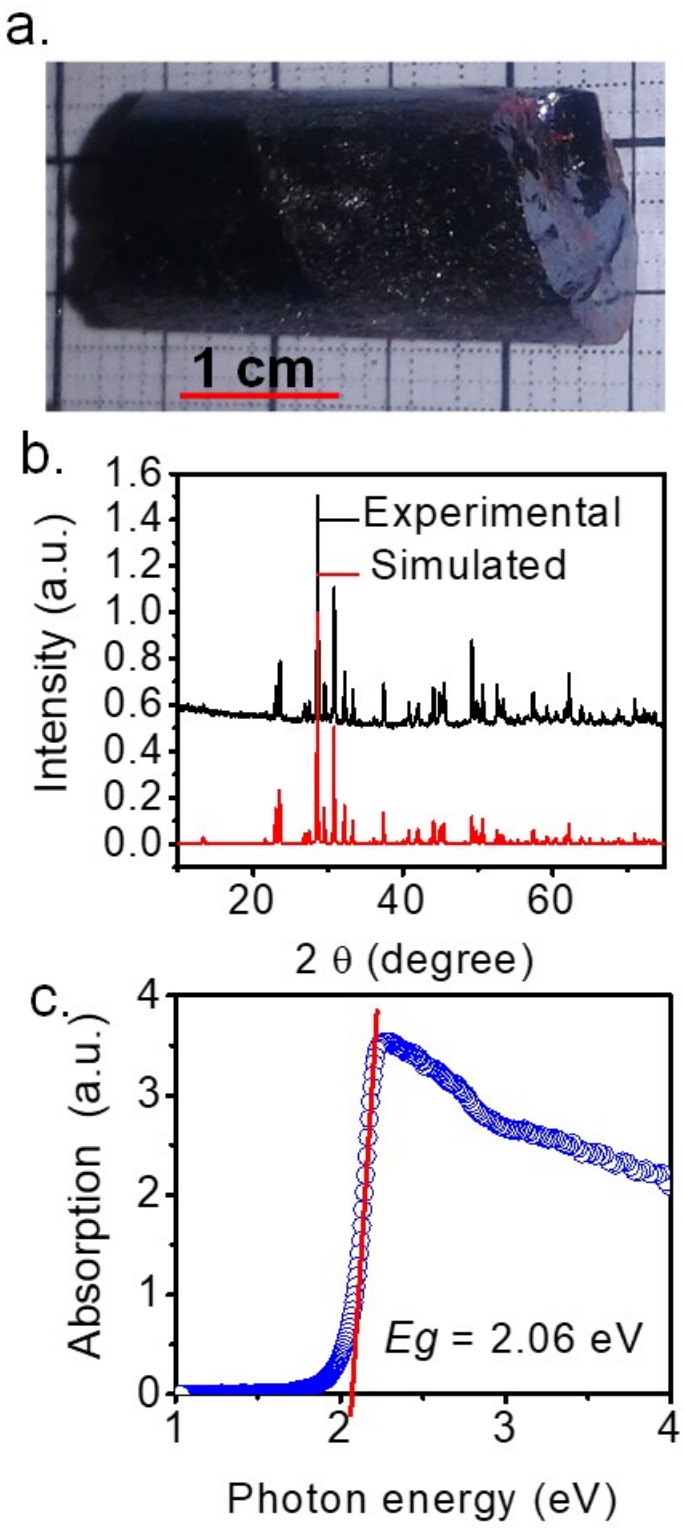


**Figure 2. (a)** Photo of $Tl_6SI_4$ pristine crystal under regular lab light. **(b)** PXRD pattern of a powdered specimen from as-grown single crystal. **(c)** Optical absorption spectrum of $Tl_6SI_4$.

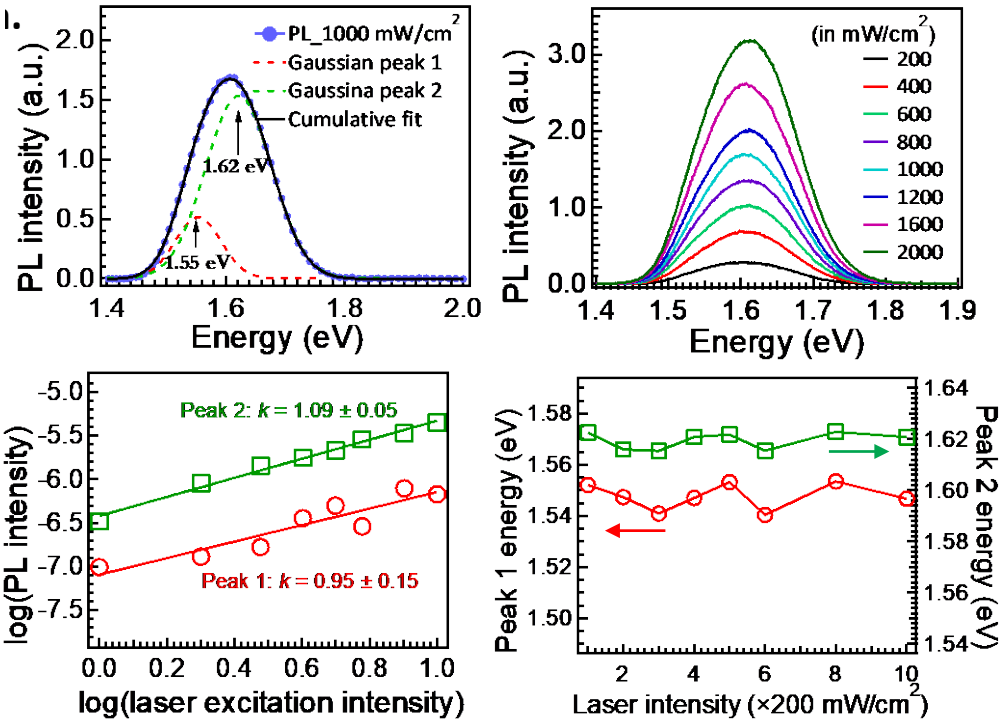


**Figure 3**. **(a)** A representative photoluminescence spectrum from a $Tl_6SI_4$ crystal collected using a laser intensity of 1000 mW·cm$^{-2}$ at 17 K **(b)** Excitation intensity-dependent photoluminescence spectra measured at 17 K. **(c)** Plots of log(photoluminescence intensity) *vs.* log(incident laser intensity) for the two observed peaks. **(d)** Corresponding plots of dependence of peak energies on laser intensity.

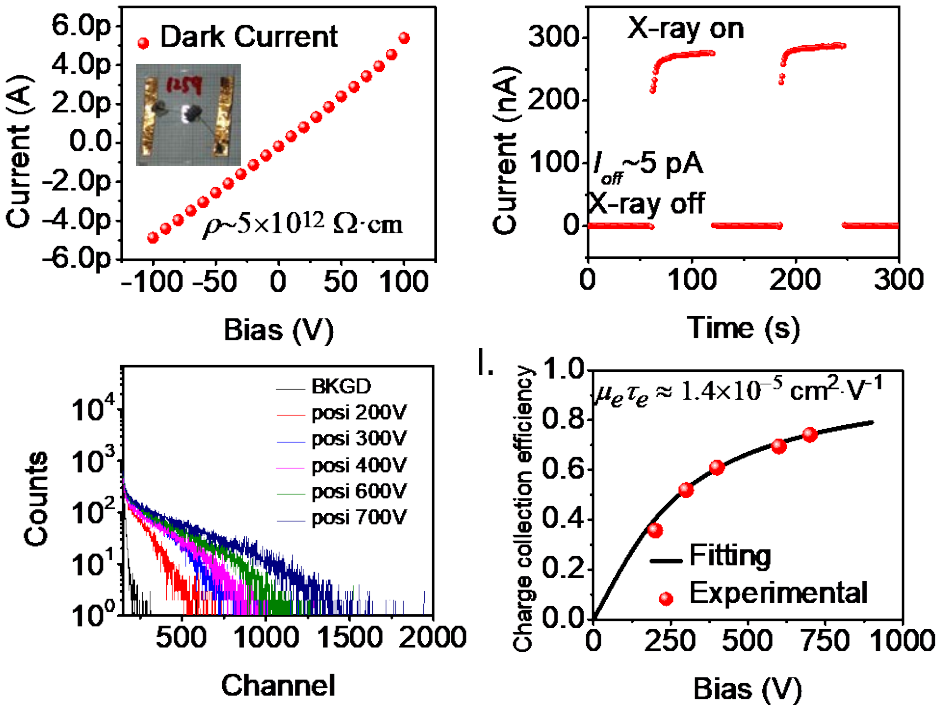


**Figure 4. (a)** *I-V* characteristic of detector made of a $Tl_6SI_4$ wafer with a thickness of 0.8 mm. The inset is the planar detector device with carbon paint electrodes. **(b)** Photoconductivity response to Ag X-rays by turning on or off the X-ray radiation source at an applied bias of 100 V. The ON-OFF ratio of current is 50000:1. **(c)** 122 keV $\gamma$-ray pulse height spectral response of $^{57}Co$ at different applied voltages. The curve "BKGD" refers to the background noise of pulse height spectrum at 700 V. **(d)** $\mu_e\tau_e$ estimation based on $\gamma$-ray spectroscopy measurements by fitting the single-carrier Hecht equation.

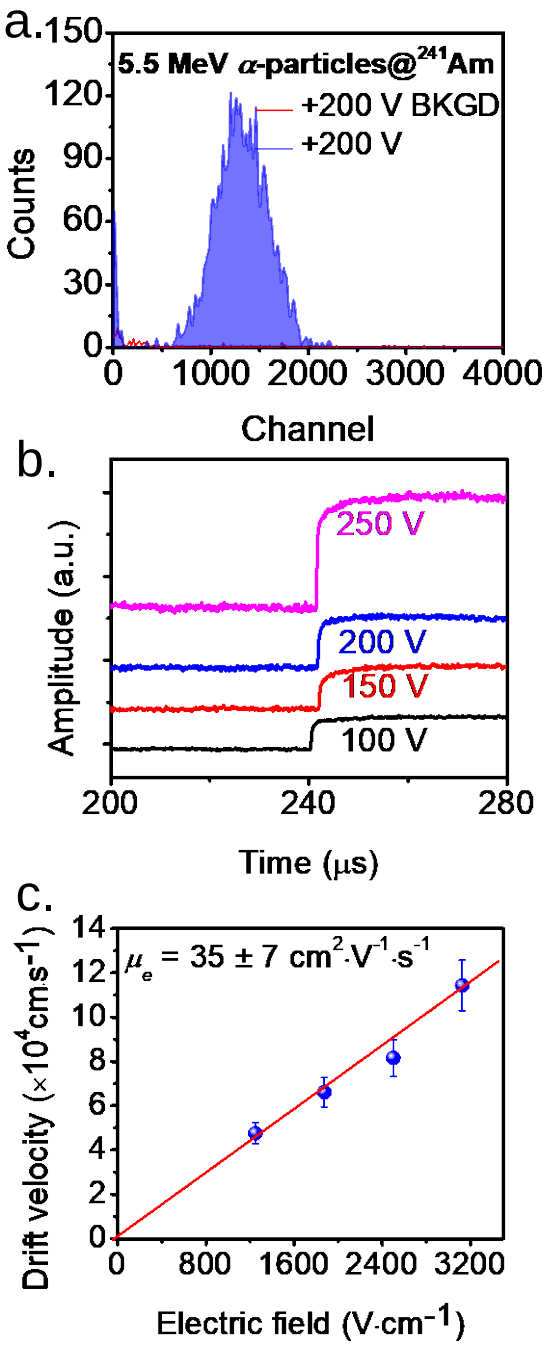


**Figure 5. (a)** $^{241}$Am $\alpha$-particles spectral response of $Tl_6SI_4$ detector at a bias of 200 V under electron-collection configuration. **(b)** Typical $\alpha$-particle induced output pulse shapes recorded by the preamplifier at different applied biases. **(c)** The dependence of electrons drift velocity on the electric field intensity of $Tl_6SI_4$ detector.

For Table of Contents Use Only

# Purification and Improved Nuclear Radiation Detection of $Tl_6SI_4$ Semiconductor

Wenwen Lin,[†,※] Zhifu Liu,[‡] Constantinos C. Stoumpos,[†] Sanjib Das,[‡] Yihui He,[†] Ido Hadar,[†] John A. Peters,[‡] Kyle M. McCall,[†,‡] Yadong Xu,[†] Duck Young Chung,[※] Bruce W. Wessels,[‡] and Mercouri G. Kanatzidis[†,*]

[†]Department of Chemistry and [‡]Department of Materials Science and Engineering, Northwestern University, Evanston, Illinois 60208, United States

[※]Materials Science Division, Argonne National Laboratory, Lemont, Illinois 60439, United States

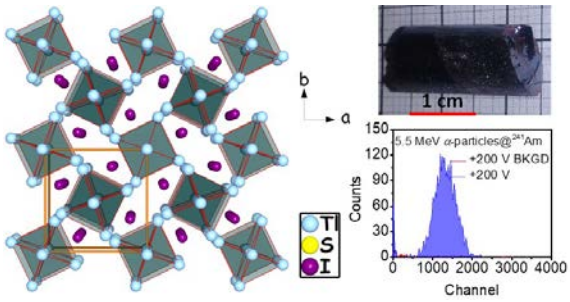


The semiconductor $Tl_6SI_4$ with high photon stopping power is a robust candidate for high-flux X-ray detection. We report effective purification protocols, impurity analysis followed by synthesis and crystal growth, charge transport and detector performance of large-size $Tl_6SI_4$ crystals. After material purification, the detector made of $Tl_6SI_4$ crystal shows promising photoresponse under Ag K$\alpha$ X-rays (22.4 keV) and $\gamma$-rays (122 keV) from $^{57}$Co.

# Supporting Information

## Purification and Improved Nuclear Radiation Detection of $Tl_6SI_4$ Semiconductor

Wenwen Lin,[†,※] Zhifu Liu,[‡] Constantinos C. Stoumpos,[†] Sanjib Das,[‡] Yihui He,[†] Ido Hadar,[†] John A. Peters,[‡] Kyle M. McCall,[†,‡] Yadong Xu,[†] Duck Young Chung,[※] Bruce W. Wessels,[‡] and Mercouri G. Kanatzidis[†,*]

[†]Department of Chemistry and [‡]Department of Materials Science and Engineering, Northwestern University, Evanston, Illinois 60208, United States

[※]Materials Science Division, Argonne National Laboratory, Lemont, Illinois 60439, United States

**Impurity analysis.** Impurity analysis was conducted on S, TlI and $Tl_2S$ before and after purification by using GDMS. The sample was ground into small pieces and mixed with trace-amount high-purity indium metal to increase electric conductivity for glow discharge.

**Photoluminescence measurement.** The photoluminescence (PL) of $Tl_6SI_4$ compound was carried out at 17.5 K. The sample was cooled down using a closed-cycle He cryostat (SHI cryogenics DE-202). The excitation source was a 405-nm, continuous-wave (CW) semiconductor laser (Coherent, Inc.) with a beam diameter of ~0.8 mm and intensity controlled by a computer. The laser beam was passed through a 405-nm bandpass filter (FHWM of 10 nm, Thorlabs, Inc.) prior to illuminating the sample surface. Subsequently, a 650-nm low pass filter was used to filter the scattered and reflected laser light before the entrance slit to the monochromator. The PL spectrum was analyzed with a ¾-m SPEX grating monochromator (both entrance and exit slit widths were set at 200 $\mu$m) and the signal was detected with a R928 Hamamatsu photomultiplier tube. An optical chopper (frequency: 710 Hz) and a lock-in amplifier with phase-sensitive detection were used to improve the signal-to-noise ratio. Finally, the PL spectra were recorded at a rate of 0.5 $nm \cdot s^{-1}$.

**Mechanical property assessment (hardness).** The Vickers hardness measurements were performed on a Struers Duramin 5 automated micro hardness test setup. As shown in Equation 1, the Vickers hardness can be derived by dividing the kgf load by the square mm area of indentation.

$$HV = \frac{2F\sin\frac{136^{o}}{2}}{d^{2}} \quad (1)$$

*F* is the load in kgf, and *d* is the arithmetic mean of the two diagonals, *d1* and *d2* in mm.

**Device fabrication.** The polished wafer with a dimension of $5 \times 4 \times 0.8$ $mm^3$ was rinsed using acetone before fabricating the planar-type detector device. One-square inch glass was used as the substrate for mounting the wafer. Electrodes of 1.5 mm in diameter were formed on the top and bottom surfaces of the wafer by applying carbon paint. Subsequently, Cu wires of 0.1 mm diameter were bonded to the electrodes and Cu foil strips attached to the insulating glass substrate.

**Charge transport and X-ray photocurrent measurements.** The current-voltage (*I-V*) measurements under dark were performed in a home-built setup. DC conductivity was collected by using a Keithley 6517B multimeter equipped with a Keithley 6105 resistivity adapter. In order to estimate the photoconductivity under X-ray irradiation, photoconductivity measurements were carried out using 22.4 keV Ag X-rays as the radiation source.

**Ambient pressure photoemission spectroscopy measurements.** The valance band maximum (VBM） energy (VBM) of a $Tl_6SI_4$ single crystal, was measured by Photoemission spectroscopy in air (PESA, AC-2, Riken-Keiki). Briefly, the sample is scanned by tunable monochromatic ultraviolet light (UV,

4.2 - 6.2 eV), under ambient conditions and the number of generated photoelectrons are measured at each excitation energy. Photoelectrons are only generated when the photon energy is higher than the VBM. The VBM is determined by finding the onset of the PESA spectra.

**Hard radiation energy spectroscopy.** Spectrometric detection performance of the $Tl_6SI_4$ detector was collected using a custom system equipped with an eV-550 preamplifier box, a spectroscopy amplifier (ORTEC, Model 572A) and a computer-installed multichannel pulse height analyzer (Model ASPEC-927). The final electronic signals were input into the MAESTRO-32 software. Spectroscopy measurements under irradiation from 122 keV $\gamma$-rays were conducted in air. The optimal linear amplifier gain, amplifier shaping time and the counting time are 500, 0.5 μs and 180 s, respectively, for $\gamma$-ray spectral response tests. An $^{241}$Am alpha sources without collimation with an activity of 0.9 μCi was used to induce the detector radiation response under 5.5 MeV $\alpha$-particles. The optimal linear amplifier gain, amplifier shaping time and the counting time are 50, 2.0 μs and 180 s, respectively. All of the measurements were performed under the electron-collection configuration. Pulse height spectra under dark were also collected as background noise under the same experimental settings. For drift mobility measurements, a homemade interface based on National Instruments software with a maximum time resolution of 4 ns to extract the complete transient waveforms from the preamplifier. The rise time of the transient waveform corresponds to the carrier drift time between 10% and 90% of the amplitude of the transient pulse.

**Table S1.** The temperatures settings for the hot and cold zones in the two-zone furnace and melting and boiling points of S and TlI precursors.

| Precursor | Nominal purity from producer | Temperature for hot zone (°C) | Temperature for cold zone (°C) | Temperature gradient estimated (°C·cm$^{-1}$) | Melting point (°C) | Boiling point (°C) |
|---|---|---|---|---|---|---|
| S | 99.999%, Alfa Aesar | 450 | 200 | 10 | 115 | 444 |
| TlI | 99.999% | 860 | 530 | 15 | 442 | 823 |

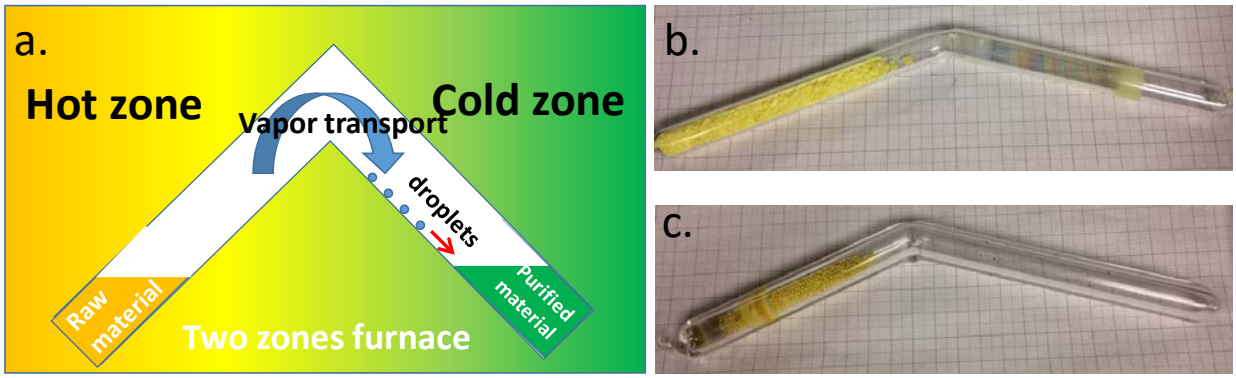


**Figure S1. (a)** The principle of evaporation method in the bent tube method of purification of S and TlI precursors. The vapor is transported due to temperature gradient, and then condenses as droplets which accumulate in the other end of bent tube. **(b)** The bent tube loaded with S precursor to be purified. **(c)** The bent tube loaded with TlI precursor to be purified. This bent geometry was found to be clearly superior to a straight tube geometry in speed and effectiveness of impurity removal.

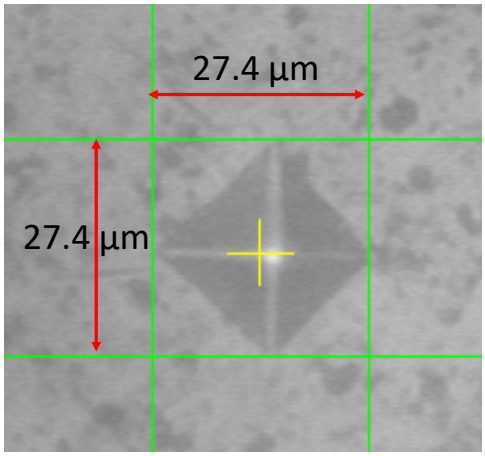


**Figure S2.** Vickers hardness measurement indents on polished $Tl_6SI_4$ wafer.

Photoemission spectroscopy in air (PESA, AC-2, Riken-Keiki), was utilized to determine the valance band maximum energy (VBM). In PESA the sample is illuminated by tunable monochromatic UV light under ambient conditions. A UV photon with energy higher than the VBM, can ionize an electron into the vacuum level. This electron can ionize a gas molecule near the surface which can be measured by the detector. For a typical measurement the energy of the photons varies between 4.2 eV to 6.2 eV and the number of generated photoelectrons is measured for each energy, this value is corrected according to the UV lamp spectrum. For semiconductors the intensity of photoemission near the VBM is generally increases as a cube root of the energy. Hence the cube root of the corrected PESA spectrum is plotted against the photon energy. The linear region of the plot above the onset is fitted to find the VBM energy, at the crossing of the fit and the background level. The conduction band minimum energy (CBM), is calculated by subtracting the measured band gap from the VBM

energy.

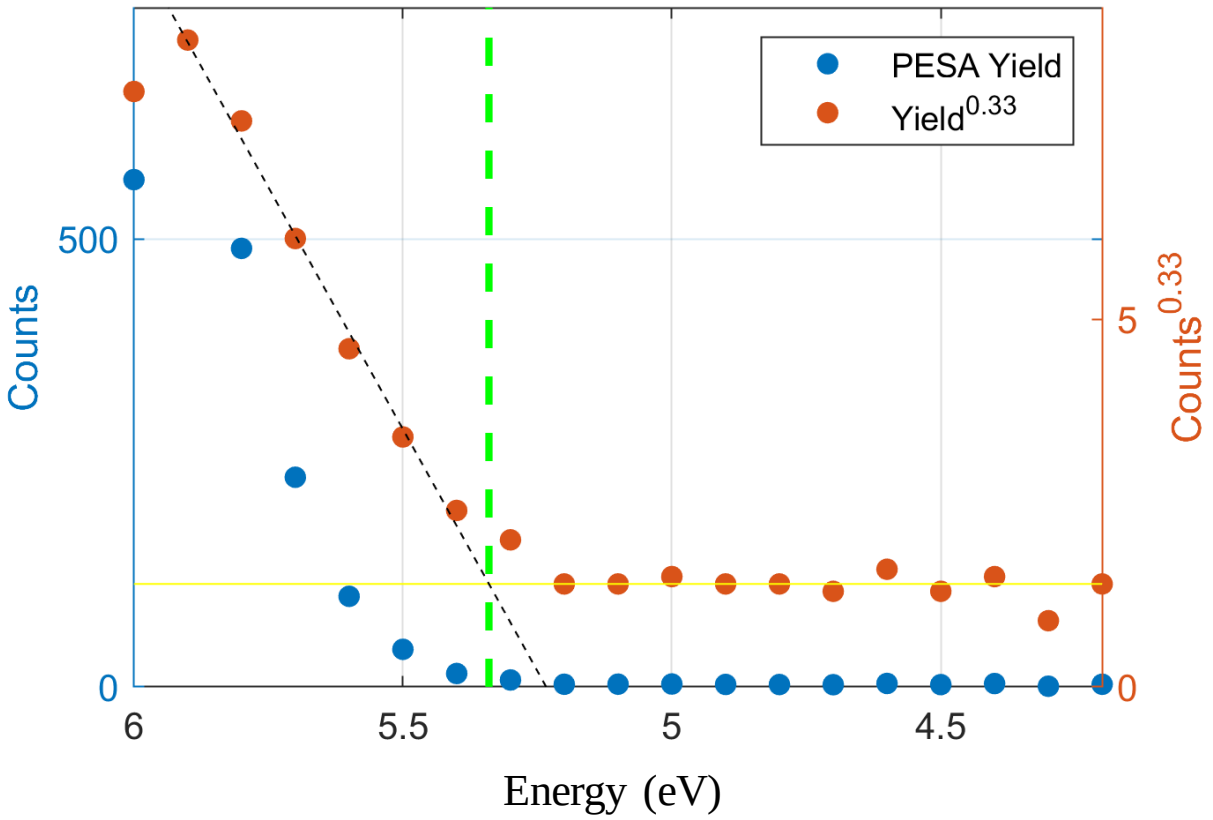


**Figure S3.** Ambient pressure photoemission spectroscopy measurement of a single crystal $Tl_6SI_4$ – Blue curve (black dots) – measured and corrected (raw – uncorrected) photoemission counts. Red curve – cube root of the photoemission counts. Yellow line marks the cube power of the background. Green markers – linear region above the spectrum onset used for the linear fit (black dashed line). Dashed yellow marker – VBM energy – intersect between the fit and the background.